ORIGINAL ARTICLE

lajss.org
Latin American Journal of Solids and Structures

www.lajss.org

Investigation of the resistance capacity of the right-angle truss-type shear connector using finite element method

Paulo Henrique Roberto Moura[a], Ramon Silva[a], Jerfson Moura Lima[b]*, Luciano Mendes Bezerra[a], Gustavo Henrique Silva Rodrigues[b], Eric Mateus Fernandes Bezerra[c]

[a]Univeristy of Brasilia, Brasília, DF, Brazil. Email: phrmoura035@gmail.com, ramon.silva@unb.br, lmbz@unb.br
[b]Federal University of Ceara, Russas, CE, Brazil. Email: jerfson.lima@ufc.br, gustavosilva@alu.ufc.br
[c]Federal University of Campina Grande, Pombal, PB, Brazil. Email: eric.mateus@professor.ufcg.edu.br

*Corresponding author

https://doi.org/10.1590/1679-78258266

Abstract

Composite structures have been successfully used in the construction of bridges and buildings as they present notable structural and constructive advantages over traditional reinforced concrete and steel systems. In steel-concrete composite beams, the joint action of the beam with the slab – which aims to exploit the main virtues of the two materials – is guaranteed by shear connectors. The stud-bolt is currently the most used connector in the world. However, the need to use specific equipment for welding makes its use difficult, especially on remote construction sites. To offer an alternative with good structural performance, low cost and easy execution, the Truss-Type shear connector was developed. In this study, a methodology was developed to numerically simulate the mechanical behavior of the Right-angle Truss-Type shear connector. Therefore, a parametric study was carried out in order to evaluate the influence of varying the connector height on its resistance. The results indicated that the use of linear finite elements in connector modeling provides good results and a significant reduction in computational cost.

Keywords

Composite beams. Push-out test. Numerical modeling. Low-cost shear connector.

Graphical Abstract

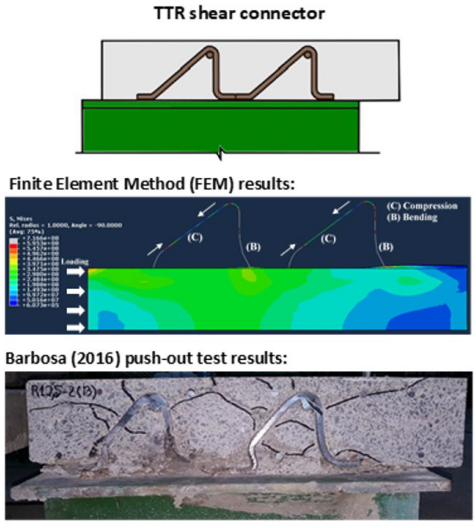

Received: jul. 3, 2024. In revised form: ago. 29, 2024. Accepted: set. 19, 2024. Available online: set. 20, 2024
https://doi.org/10.1590/1679-78258266

1 INTRODUCTION

The increase in demands regarding productivity, efficiency and sustainability in the construction industry has stimulated the search for alternative structural systems to those traditionally used in Brazil. In addition to meeting the aforementioned requirements, Lacki et al. (2019) states that composite steel-concrete systems can provide more economical solutions than steel ones and lighter than reinforced concrete ones. Composite steel-concrete systems also present advantages that are characteristic of prefabricated systems, such as: reducing the use of formwork and shoring, obtaining a lean construction site, reducing material waste and improving quality and performance degree of confidence of the structure.

Steel-concrete composite beams are formed by the association of a concrete slab supported on a steel profile. These elements are joined by so-called shear connectors in order to explore the main virtues of each material. Therefore, the joint action of the elements must produce predominantly compressive stresses in the concrete and tensile stresses in the steel.

Although composite steel-concrete beams have been widely used in the construction of buildings and bridges for decades (Han et. al., 2017), the adoption of this system by the Brazilian market is still below its potential, especially in medium and small projects size. One of the main factors for this is the cost of shear connectors. The stud bolt – which is the most used shear connector in composite structures (Bonilla et al., 2019) – has a high cost as it is imported and patented (Lima, 2021). Furthermore, high productivity in its installation – which is one of the factors that justifies its preference (Kim et al., 2016) – is only achieved by a welding process that requires the use of high-power generators (Bezerra et al., 2018).

In this context, the Truss-Type (TT) shear connector was developed within the scope of the University of Brasília (UnB) (Bezerra et al., 2018). It is composed of CA-50 steel bars (yield strength of 500 MPa) used in reinforced concrete structures, bent into a triangular shape and fixed to the steel profile flange by common welding. A bar 40 mm long and 16 mm in diameter is welded to the top apex of the connector to improve its efficiency in restricting transverse separation. The TT shear connector was registered with the National Institute of Industrial Property (INPI) under number BR302016002949-0. As shown in Figure 1, two geometries were proposed: Isosceles Truss-Type connector (TTI) and Right-Angle Truss-Type connector (TTR).

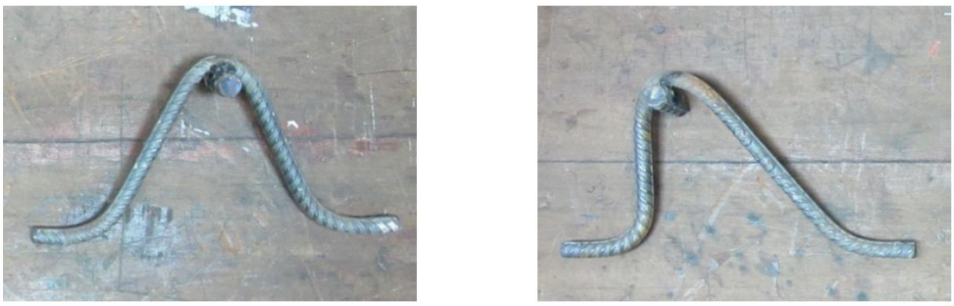

(a) TTI connector (b) TTR connector

Figure 1 Truss-Type shear conector, Barbosa (2016)

The studies carried out by Barbosa (2016), Bezerra et al. (2018), Lima et al. (2020), Lima et al. (2022) and Lima et al. (2024) showed that the TT shear connector presents good structural performance when compared to the stud bolt. Furthermore, its use becomes attractive because it is made with low-cost material that is easily found on the market, welding can be done with common electrodes and machines and the manufacturing process is simple and reasonably mastered.

Barbosa (2016) carried out the push-out test on 24 models of composite beams with solid concrete slabs. For comparison, 3 of these models were made with stud bolt connectors measuring 19 mm in diameter and 130 mm in height. The other models were made for TTI and TTR connectors with 8 mm, 10 mm and 12.5 mm diameter bars. As with the stud bolt, 3 push-out models were made for each configuration. The results showed that all TT connectors tested are ductile and presented a higher shear resistance/cross-sectional area ratio than the stud bolt.

The results of the 12.5 mm diameter TTI connector were compared to the stud-bolt results and published in Bezerra et al. (2018). In addition to the experimental results, a methodology for numerical modeling in non-linear finite elements was presented that simulates the results of the push-out test with good accuracy. Using this methodology, Lima et al. (2020) developed a parametric study of the TTI connector. The variation of geometric parameters (height, opening angle between the inclined legs and connector diameter) and the concrete strength of the slab were evaluated. From the results, a non-linear regression was applied to obtain an equation capable of estimating the resistance capacity

of the TTI connector with 90 mm height and 80° opening (best geometry) as a function of the concrete strength of the slab and the diameter of the connector.

A finite element model was developed by Lima et al. (2022) to simulate the push-out test carried out by Barbosa (2016) for the TTR connector. From this model, it was possible to verify that arranging the TTR connector in an orientation opposite to that defined by Barbosa (2016) (Figure 2) provided an increase of 17.86% in shear resistance for the 12.5 mm diameter. The improvement in performance occurred because the change in direction in relation to the load promoted an inversion of the load on the inclined leg (which began to be pulled instead of compressed). For the TTR connector with inverted direction (TTR-I), a parametric study was carried out, varying only the connector diameter and the concrete strength, and an equation to estimate the shear resistance was also obtained.

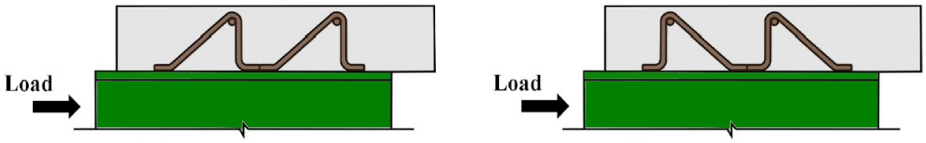

(a) TTR connector (b) TTR-I connector

Figure 2 TTR shear connector application guidelines on steel I-beam, Lima et al. (2022)

The first study of the performance of the TT connector in a full-scale steel-concrete composite beam was carried out by Lima et al. (2024). In this work, an experimental bending test was carried out on three beams simply supported with TTI connectors. The beams tested showed different degrees of connection. The results showed that there is an increase in the beam's resistance capacity the greater the degree of connection. However, this increase was not proportional; the beam with connection degree 1.06 presented resistance only 21.07% higher than the beam with connection degree 0.47. Furthermore, it was possible to verify that the equation for predicting the resistance of the TTI connector obtained in Lima et al. (2020) is efficient.

As previously described, the approach based on the Finite Element Method (FEM) has been successfully used to study the behavior of the TT connector. However, it is worth highlighting that the use of three-dimensional elements and the consideration of all sources of non-linearities in materials and contact between elements make numerical models robust and have a high computational cost. Even using computers with high processing power, it takes a lot of time to simulate each model, making a more extensive parametric study difficult.

With the aim of presenting an alternative methodology that offers lower computational cost, but is capable of numerically simulating the push-out test with good precision, this work will investigate the feasibility of using linear finite elements in modeling the TTR connector. The results of the experimental tests carried out by Barbosa (2016) will be used to calibrate and validate the numerical model. After validation, a study will be carried out on the effect of height variation on the resistance capacity of the TTR connector and a comparison with the results obtained by Lima et al. (2020) for the TTI connector.

2 BARBOSA (2016) PUSH-OUT TEST

Barbosa (2016) carried out push-out tests in accordance with the prescriptions of the European Code EN 1994-1-1:2004 to compare the performance of TTI and TTR connectors with stud bolt. In this test, an A36 steel profile with section I W250x73 is connected by shear connectors to two solid slabs made of concrete with an average compressive strength of 34 MPa. The slabs are reinforced with 10 mm diameter CA-50 steel bars. It should be noted that, to accommodate the TT connectors, it was necessary to increase the height of the specimen by 10 cm – and a layer of reinforcement – in relation to the dimensions specified in EN 1994-1-1:2004 (Eurocode-4, 2004). Figure 3 shows the geometric details of the specimens with TTR connector.

The slip displacements (relative longitudinal slip between the steel profile and the concrete slabs) and uplift (the transverse separation of the slabs in relation to the steel profile) were measured by LVDTs (Linear Variable Differential Transformer) as a progressive force P was applied in the steel profile. This application was carried out using a hydraulic actuator (coupled to a test gantry) and the force intensity was controlled using a load cell with a capacity of 2000 kN. Electrical resistance strain gauges were attached to the connectors to monitor specific strains. The load, slip and strain values were read by the Spider 8 data acquisition modules (model SR30) and recorded in the Catman software, version 4.5 from HBM. Figure 4 shows details of the experimental setup.

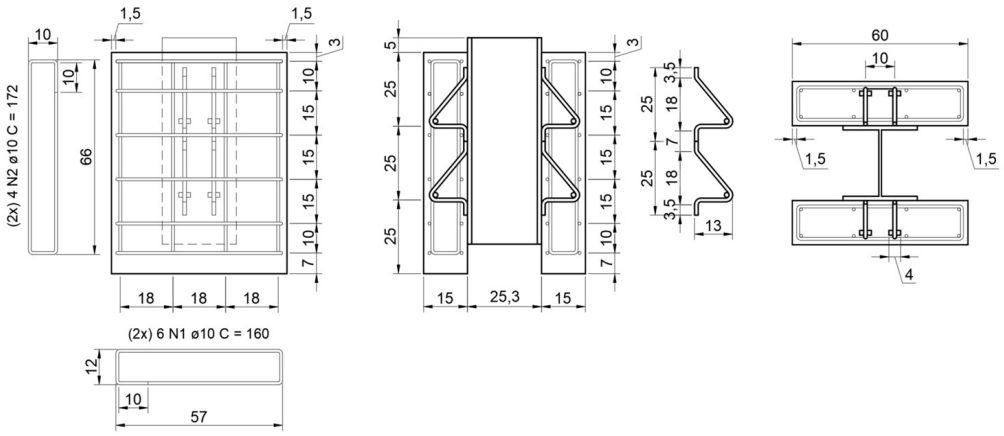

Figure 3 TTR push-out test – dimensions in cm

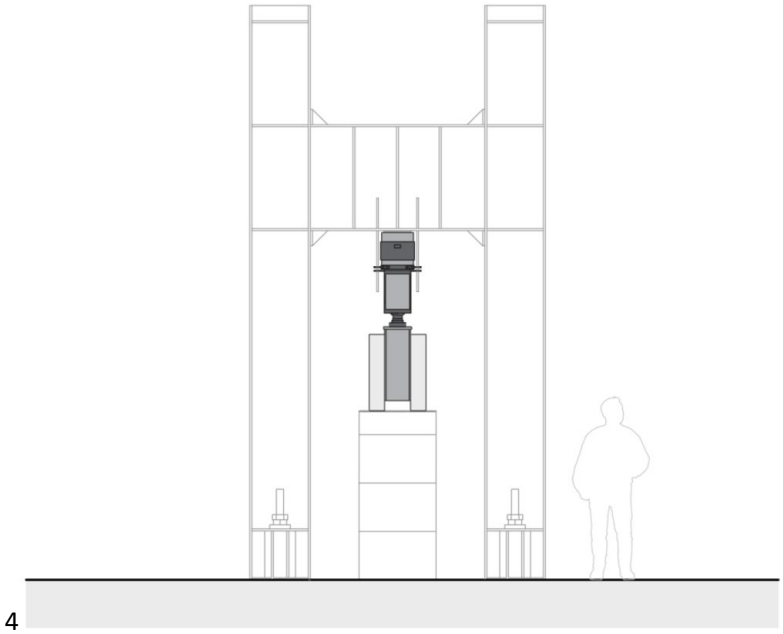

Figure 4 Experimental setup

From the load-slip curve produced by the test, it was possible to define the resistance capacity and ductility of the connector. The TTR connector with 12.5 mm in diameter showed ductile behavior and an average resistance of 173.01kN, which is higher than that presented by the stud bolt (124.63 kN), however, lower than the TTI connector with the same diameter (194.14 kN). It should be noted that unlike the stub bolt, in which the failure led to the slab detachment, the TTR connector failed without the slab detachment occurring.

3 NUMERICAL MODEL

The non-linear three-dimensional numerical model was constructed using the finite element method (FEM) within the ABAQUS 6.14.1 software. This model accounts for material nonlinearities in both steel and concrete, as well as their interactions. To maintain symmetry and expedite processing, only one-quarter of Barbosa's (2016) experimental model was simulated, ensuring consistent results through imposed boundary conditions. The model comprises several components: steel I profile, concrete slab, TTR connector, and slab reinforcement, all designed to replicate the geometry described by Barbosa (2016), as illustrated in Figure 3.

3.1 Constructive model for concrete

ABAQUS 6.14.1 have the Concrete Damaged Plasticity (CDP) constitutive model available in its library. This model is ideal for materials, which, such as concrete, exhibit different behaviors when subjected to compression and tension. The CDP is capable

of simulating concrete failure due to crushing, when subjected to compression and cracking, when subjected to tension. One of its notable features is its capability to capture concrete failure mechanisms, including crushing under compression and cracking under tension. By incorporating damage evolution laws, CDP can accurately simulate the progressive degradation of concrete as it undergoes loading, providing valuable insights into structural response and failure modes.
This makes CDP a valuable tool in the analysis and design of concrete structures, ensuring robust and reliable performance predictions. Other works adopted this model, such as Qureshi e Lam (2012), Qureshi, Lam e Ye (2011), Shariati et al. (2016), Xu, Su e Sugiura (2017), Bonilla et al. (2015), Lima et al. (2020), Lima et al. (2022). The same plastic parameters were adopted as the authors: Alfarah et al. (2017) and Lopez-Almansa et al. (2014), they are presented in Table 1. The parameters are: expansion angle φ, ratio between the magnitude of deviatoric stress in uniaxial tension/compression K_c, the ratio between biaxial and uniaxial compression strengths f_{b0}/f_{c0} and eccentricity of plastic potential surface ϵ.

Table 1 Plastic Parameters of CDP

φ	K_c	f_{b0}/f_{c0}	ϵ
13º	0,7	1,16	0,1

The uniaxial stress x strain curve of concrete in compression, shown in Figure 5a, is divided into 3 parts. The first corresponds to values between 0 and $0{,}4f_{cm}$, corresponding to a stretch of linear elastic behavior. The f_{cm} is the concrete's average compressive strength (Equation 1) and ε_{cm} is the corresponding deformation chosen from the FIB Model Code 2010 (2012). E_{ci} is the initial elastic modulus (Equation 2). And E_0 is the secant modulus of elasticity of the concrete (Equation 3). The behavior of the section between 0 and $0{,}4f_{cm}$ is governed by equation (4) FIB Model Code 2010 (2012).

$$f_{cm} = f_{ck} + 8 \tag{1}$$

$$E_{ci} = 10000 f_{cm}^{\frac{1}{3}} \tag{2}$$

$$E_0 = \left(0{,}8 + 0{,}2\frac{f_{cm}}{88}\right) E_{ci} \tag{3}$$

$$\sigma_{c(1)} = E_0 \varepsilon_c \tag{4}$$

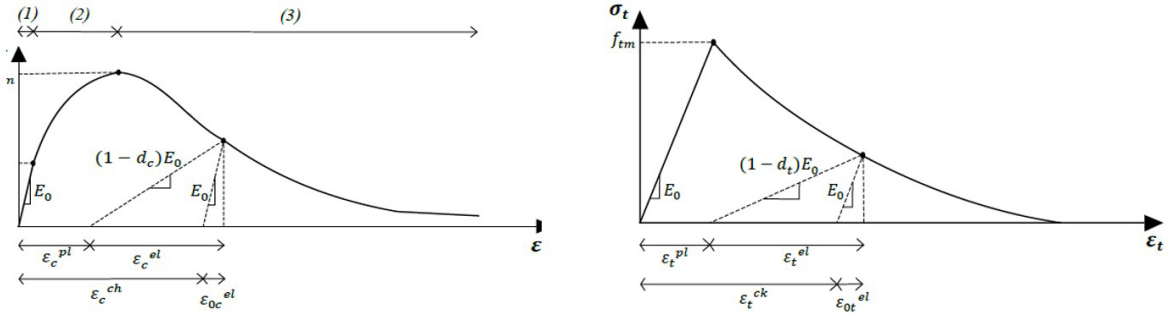

Figure 5 Uniaxial behavior of concrete

The second region between $0{,}4f_{cm}$ and f_{cm} is governed by Equation (5). The third region describes the softening in compression developed by Krätzig and Pölling (2004) see Equation (6).

$$\sigma_{c(2)} = \frac{E_{ci}\frac{\varepsilon_c}{f_{cm}} - \left(\frac{\varepsilon_c}{\varepsilon_{cm}}\right)^2}{1 + \left(E_{ci}\frac{\varepsilon_{cm}}{\varepsilon_{cm}} - 2\right)\frac{\varepsilon_c}{\varepsilon_{cm}}} f_{cm} \tag{5}$$

$$\sigma_{c(3)} = \left(\frac{2 + \gamma_c f_{cm} \varepsilon_{cm}}{2 f_{cm}} - \gamma_c \varepsilon_c + \frac{\varepsilon_c^2 \gamma_c}{2\varepsilon_{cm}}\right)^{-1} \tag{6}$$

$$\gamma_c = \frac{\pi^2 f_{cm}\varepsilon_{cm}}{2\left[\frac{G_{ch}}{l_{eq}} - 0{,}5 f_{cm}\left(\varepsilon_{cm}(1-b) + b\frac{f_{cm}}{2\varepsilon_{cm}}\right)\right]^2} \tag{7}$$

$$b = \frac{{\varepsilon_c}^{pl}}{{\varepsilon_c}^{ch}} \tag{8}$$

In Equation (7) G_{ch} corresponds to the concrete crushing energy per area and l_{eq} is the length of the finite element adopted in the numerical model. In Equation (8) ε_c^{pl} is the plastic deformation and ε_c^{ch} is the crushing deformation. The parameter γ_c (Equation 6) is responsible for controlling the area under the curve (third section). According to Krätzig and Pölling (2004), the area under the curve must be equal to the localized crushing energy, given by the relationship G_{ch}/l_{eq}. The ultimate compressive strain of concrete is defined so that the restriction discussed above is met. $b = 0{,}9$ was adopted (Alfarah et al. 2017), by calculating ε_c^{pl} l and ε_c^{ch} a new value of b is obtained and compared with the initial value. An iterative process is applied until convergence is achieved.

The uniaxial tensile behavior (Figure 5b) is defined in two regions, the linear elastic one governed by E_0 and the second region is governed by the fracture energy according to Cornelissen et al. (1986), this can be seen in Figure 6.

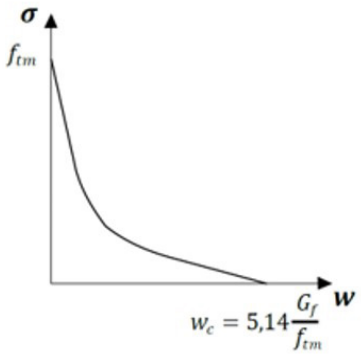

Figure 6 Softening in tension in terms of fracture energy

In Figure 6, f_{tm} corresponds to the average tensile strength, G_f is the fracture energy per unit area and w_c is the critical fracture opening. According to the fib Model Code 2010 (2012), f_{tm} and G_f are defined according to Equations (9) and (10).

$$f_{tm} = 0{,}3016 {f_{ck}}^{2/3} \tag{9}$$

$$G_f = 0{,}073 {f_{cm}}^{0{,}18} \tag{10}$$

Based on the fracture energy, Oller (1988) defines the concrete crushing energy (G_{ch}) as per Equation (11). Cornelissen et al. (1986) proposed equation (12) that describes the traction softening behavior. The following boundary conditions can be seen for this equation $\sigma_t(0) = f_{tm}$ and $\sigma_t(w_c) = 0$, conditions that were already expected, the first states that when the crack opening is minimum the concrete resistance is maximum. The second condition implies that if the opening is maximum, the resistance is minimum. Even though the values of c_1 = 3 and c_2 = 6,93 according to Cornelissen et al. (1986).

$$G_{ch} = \left(\frac{f_{cm}}{f_{tm}}\right)^2 G_f \tag{11}$$

$$\frac{\sigma_t(w)}{f_{tm}} = \left[1 + \left(c_1 \frac{w}{w_c}\right)^3\right] e^{-c_2\frac{w}{w_c}} - \frac{w}{w_c}(1 + {c_1}^3)e^{-c_2} \tag{12}$$

The critical crack opening w_c is calculated according to Equation (13). As the loss of tensile strength is a function of the opening of cracks in the concrete, it is possible to state that softening can also be defined as a function of the deformation of the concrete. According to Alfarah, López-Almansa and Oller (2017), the strain values that define the

second section of the stress x strain relationship in Figure 5b can be obtained by Equation (14). In this same equation ε_{tm} is the deformation corresponding to the average tensile strength ε_{tm}.

$$w_c = 5{,}14\frac{G_f}{f_{tm}} \tag{13}$$

$$\varepsilon_t = \varepsilon_{tm} + \frac{w}{l_{eq}} \tag{14}$$

Table 2 shows the concrete properties considered for the numerical model. These mechanical properties were determined to by Barbosa (2016), in material characterization tests.

Table 2 Mechanical properties of concrete

E_o (GPa)	f_{cm} (MPa)	f_{tm} (MPa)
26.0	34.0	3.6

3.2 Constitutive model for steel

To model the steel in this study, an elastic-plastic constitutive model with isotropic flow was used. It is available in the ABAQUS material library, under the name PLASTIC. According to Barbosa (2016), throughout the execution of the push-out test, the steel profiles remained in the elastic regime. Therefore, for the steel profile only the elastic properties were considered: Modulus of elasticity (E_s) with a value of 210 GPa and Poisson's ratio of 0.3. For the other components (TTR connectors and slab reinforcement), a linear elastic-plastic behavior was considered, given the high stress levels in these components.

For the shear connectors, a tri-linear behavior was adopted (Figure 7a), the most important component of the model. The bi-linear behavior (Figure 7b) was adopted for the slab reinforcement steel. The mechanical properties of the steels used in the model were taken from Barbosa (2016), and can be viewed in Table 3. In Figure 7 and Table 3, E_s is the elastic modulus of the steel, σ_y e ε_y are the yield stress and its respective deformation, σ_u e ε_u and are the ultimate stress and respective deformation. The Poisson ratio of the steel of the TTR connectors and slab reinforcement was also adopted at a value of 0.3.

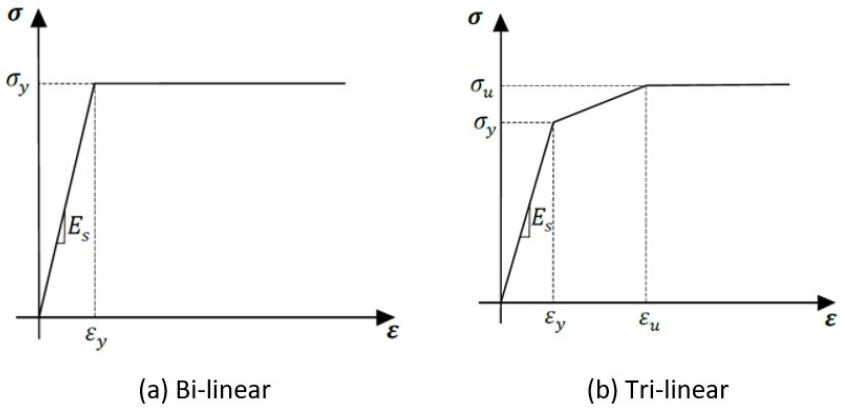

Figure 7 Uniaxial behavior of steel

Table 3 Mechanical properties of steels

Model components	E_s (GPa)	σ_y (MPa)	ε_y (%)	σ_u (MPa)	ε_u (%)
TTR connector	195.30	595.30	0.30	716.60	6.0
Slab reinforcement	198.40	561.20	0.28	663.2	6.0
Profile	210	-	-	-	-

3.3 Constraints and contact interactions

In order to guarantee the connection between the model components, appropriate contact interactions and restrictions were adopted. In the specimens by Barbosa (2016), a lubricant was applied to the surface of the steel profile flange, with the aim of reducing friction between the steel element and the concrete slab, and consequently, the TTR connectors were the main responsible in transmit efforts between components. Therefore, for the contact interaction between the steel profile and the concrete slab, a contact interaction with frictionless tangential behavior was applied. And for the normal behavior of the interaction, the "Hard" option was considered, which induces the model that one surface cannot penetrate the other. In Figure 8a, the surfaces with the described contact interaction can be seen. The connection of the TTR connector to the steel profile was carried out using the tie restriction (Figure 8b). This restriction was chosen because in tests by Barbosa (2016) it was observed that the weld that connects the TTR connector to the steel profile remained intact after the specimens ruptured.

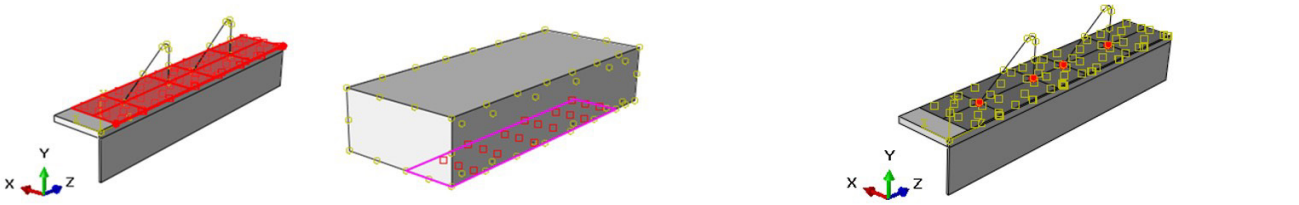

(a) Surfaces in contact interaction between steel profile flange and concrete slab

(b) Tie constraint between steel profile and connectors

Figure 8 Constraints and contact interactions

The TTR connectors and slab reinforcement were considered embedded in the concrete slab, based on the embedded region restriction. This type of restriction guarantees the joint work of the embedded elements (connectors and slab reinforcement bars) and the host region (concrete slab). In Figure 9 the application of the embedded restriction can be seen. The red color indicates the embedded elements and the margin color the host region.

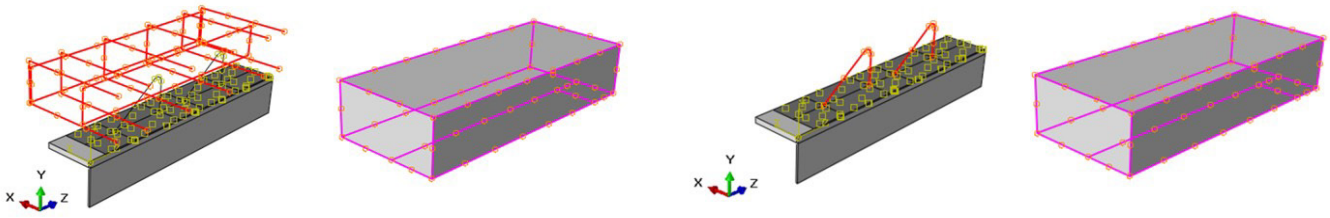

(a) Slab reinforcement

(b) Connector-concrete slab

Figure 9 Embedded constraints

3.4 Boundary conditions and loading

The applied boundary conditions were applied to the model in order to prevail geometry simplification, and to adequately simulate the push-out test. The symmetry boundary conditions consisted of restricting the displacements in the X and Y directions on surfaces 1 and 2, respectively (Figures 10a and 10b). As for the boundary condition referring to the push-out test, the displacements of the slab base (surface 3) were restricted in the Z direction (Figure 10c). The model load was applied in the Z direction, distributed uniformly in the steel profile cross-section (Figure 10d).

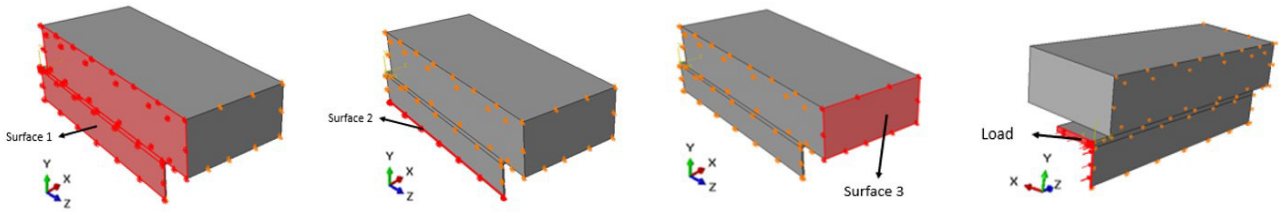

Figure 10 Loading and boundary conditions.

3.5 Analysis method

To analyze the numerical model, the dynamic explicit method was adopted. Despite being a dynamic analysis method, it can be adopted for quasi-static models, through the slow application of loading. A loading application speed was adopted so that the model's kinetic energy reached a maximum of 10% of the total internal energy, which characterizes an explicit quasi-static dynamic analysis, according to Abaqus (2014). The dynamic explicit method was adopted due to the high complexity of the model when considering the non-linearities of materials and contact interactions and also because it is efficient in analyzing material damage and large deformations. Several researchers have already used this method to model push-out tests and obtained satisfactory results (Bezerra et al., 2018; Kim et al., 2017; Nguyen and Kim, 2009; Xu et al., 2014; Zheng et al. 2019).

3.6 Mesh and types

The choice of mesh and finite elements for each component of the model was carried out so that the results were accurate. Each component was modeled separately, thus constituting independent meshes. The C3D8R element (three-dimensional hexahedral element with 8 nodes and reduced integration) was adopted for the steel profile and concrete slab. This element offers more approximate results and lower computational cost for analysis, when modeling three-dimensional geometries (Abaqus, 2014). The size of the elements was 25 mm and 10 mm for the concrete slab and the steel profile, respectively. Figure 11 shows the finite element mesh of the model.

The TTR connectors were modeled using a linear finite element, with the aim of achieving greater model efficiency, that is, accurate results and lower computational costs. The three-dimensional beam element with 2 nodes (T3D2) with size of 10 mm was adopted. To reinforce the slab, a three-dimensional truss element with 2 nodes (T3D2) was used, measuring 10 mm (see Figure 11).

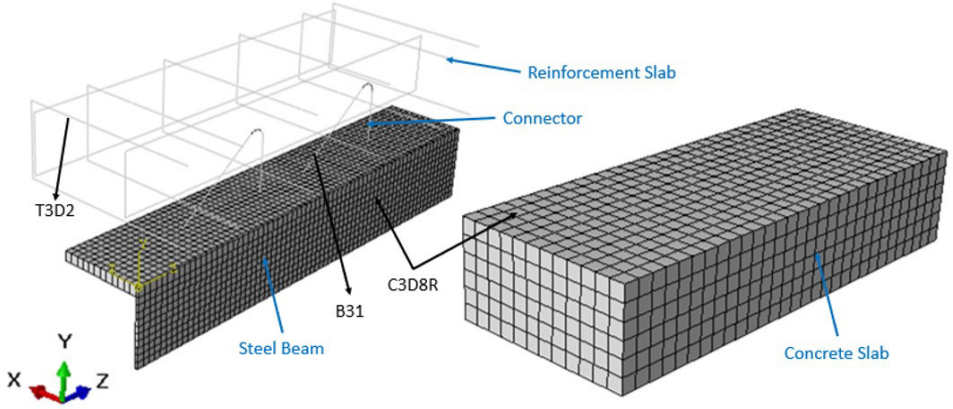

Figure 11 Mesh and types finite elements

4 VALIDATION

The developed numerical model was validated with the experimental results of Barbosa (2016). In this procedure, the resistance capacity of the TTR connector, the load x slip curves and the failure modes were verified. Figure 12 shows the comparison of the experimental load x slip curves and those obtained numerically (FEM), for the TTR connector with

a diameter of 12.5 mm. The agreement between the numerical curve and the experimental curves is notable, both for the initial loads and for the model's failure load levels. It can also be identified that the numerical curve has no loss of stiffness at the model's failure load levels, as the numerical simulation is carried out with load control. However, a flow plateau is well defined, that is, significant displacements occur for small load increments, thus indicating the failure region of the numerical model.

As a load control was adopted in the numerical simulations, the resistance capacity of the numerical model was designated as the load related to the sliding of 20.88 mm. This slip was obtained with the average of the slips referring to the ultimate loads of the experimental models. The resistance capacity of the model was divided by the number of connectors in the model to determine the resistance capacity of the TTR connector. Table 4 presents in detail the resistance capacity of the TTR connector obtained from experimental tests (P_{exp}) and finite element analysis (P_{FEM}). The biggest difference between the experimental and numerical results was 13.8%. However, the average value of P_{exp}/P_{FEM} was 0.088, with a coefficient of variation of 0.084. These results indicate that the numerical model developed is efficient in simulating the resistant capacity of the TTR connector.

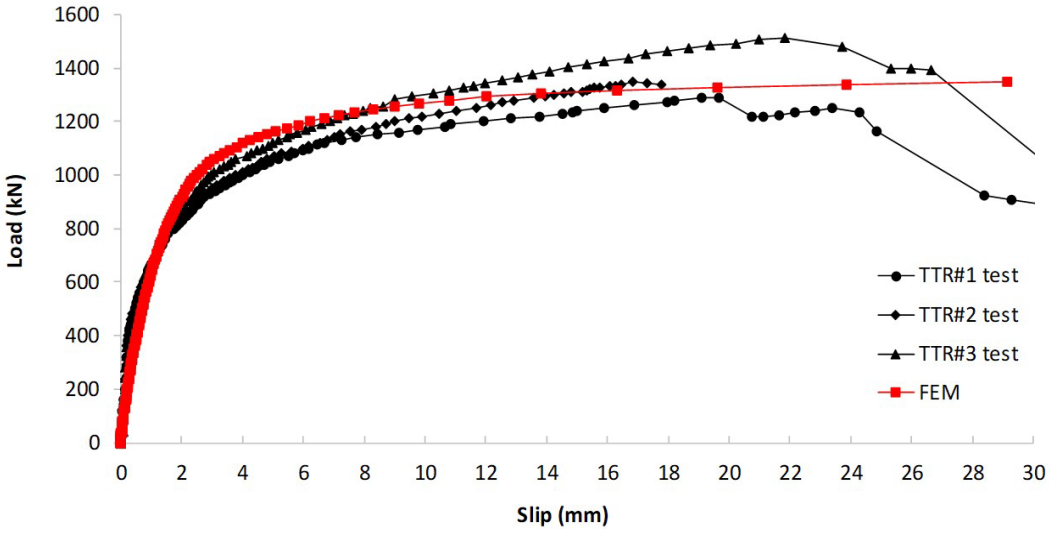

Figure 12 Load applied versus slip curves

Table 4 Resistance capacity obtained by experimental tests and FEM

Model	P_{exp} (kN)	P_{FEM} (kN)	P_{exp}/P_{FEM}
TTR#1	161.27	166.32	0.969
TTR#2	168.40		1.012
TTR#3	189.35		1.138
Mean			1.040
Coefficient of variation (CV)			0.084

Figure 13 shows the deformed configuration of the TTR connectors at the moment of the model's ultimate load. The longitudinal shear force in conjunction with the reaction of the concrete slab causes the vertical leg of the TTR connector to be subjected to bending. The inclined leg is subjected to compression efforts until instability occurs. This deformed configuration of the TTR connectors was also observed in the tests by Barbosa (2016), as can be seen in Figure 15.

Still in Figure 13, the Von Mises stress distribution in the TTR connectors can be visualized. It is noted that the highest stress levels occur in the region of the base of the connectors, stresses that are higher than the yield stress of the steel (f_y = 595.30 MPa). Figure 14 shows the stress distribution in the concrete slab, it is noted that a concentration of stress occurs in the regions close to the base of the connectors. The stress levels in the concrete exceed the compressive strength of the concrete (f_{cm} = 34 MPa). The stress analysis of the model at the moment of ultimate load indicates that the rupture of the push-out model with a TTR connector with a diameter of 12.5 mm occurs due to the association of the flow of the connector legs and crushing of the concrete slab in the regions close to connector base. This rupture mode corroborates the results of numerical simulations by Lima et al. (2022).

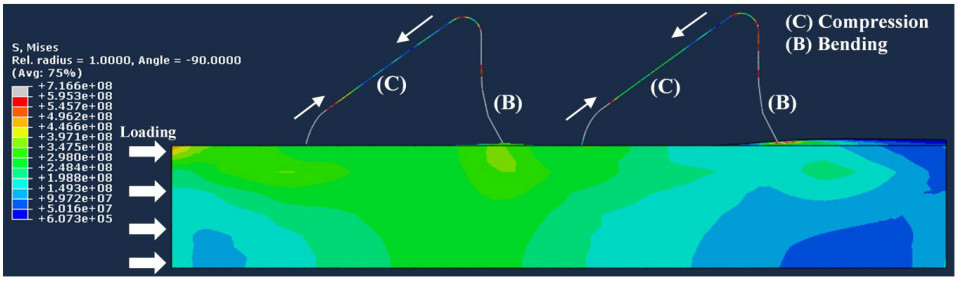

Figure 13 Deformed configuration and stress (Pa) distribution at the moment of ultimate load

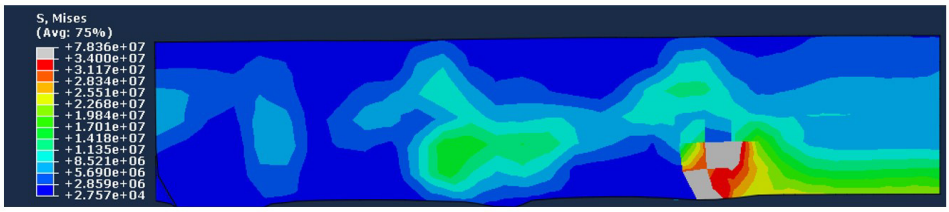

Figure 14 Stress (Pa) distribution in the concrete slab

Figure 15 Section on the TTR connectors alignment of specimen after the push-out test performed by Barbosa (2016)

Lima et al. (2022) also proposed a finite element model to simulate the behavior of the TTR connector. However, the authors used three-dimensional elements to simulate the TTR connector. Figure 16 presents the results of Lima et al. (2022) for the deformed configuration of the TTR connectors, and stress distribution in the connectors and concrete slab. A similarity is noted with the numerical results of this study. However, Lima et al. (2022) used three-dimensional elements to simulate the TTR connector, increasing the number of finite elements and degrees of freedom of the model, and consequently, increasing the computational cost. Using a computer with an Intel Core i5-2500 processor, a processing frequency of 3.5 Gigahertz, and 8 Gigabytes of RAM, the processing time of the Lima et al. (2022) model was approximately 20 hours. The processing time of the model proposed in this study was just 0.75 hours, almost 27 times shorter, using a computer with similar configurations (Intel Core i3-4005U processor, a processing frequency of 1.7 Gigahertz, and 8 Gigabytes of RAM).

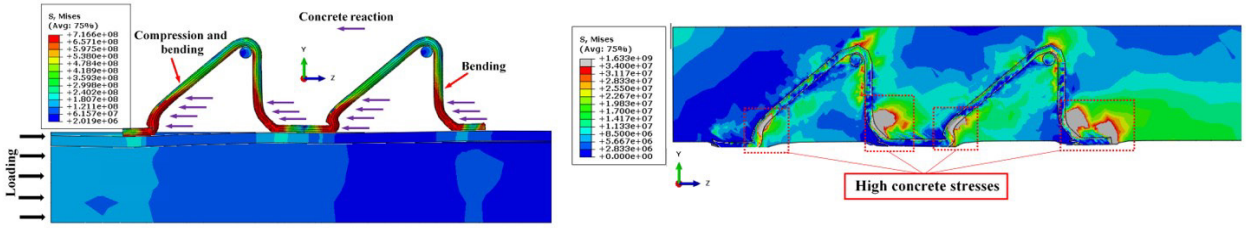

(a) Deformed and stress distribution in connectors (b) Stress distribution in the slab

Figure 16 Lima et al. (2022) model results

The results of the load x slip curve, resistance capacity and failure modes presented in this section confirm the efficiency of the finite element model proposed in this study in simulating the behavior of the TTR shear connector, with the great advantage of being a cost-effective numerical model very low computational cost when compared to other numerical models in the literature.

5 PARAMETRIC STUDY

The geometry of the TTR connector is defined by a height (h), opening angle between the legs (α), distance between the base of the legs (l_{ab}), in addition to the 35 mm long horizontal legs that are used for welding of the TTR connector on the steel profile (Figure 17). The geometric configuration of the TTR connector proposed by Barbosa (2016) has the following dimensions: h = 130 mm, α = 50° and l_{ab} = 180 mm. Despite having carried out 9 push-out tests with the TTR connector, Barbosa (2016) only investigated the influence of the connector diameter on its resistance capacity. The other parameters, such as height (h), were not evaluated. The height of the shear connector is a fundamental parameter for the behavior of the steel-concrete connection of composite structures, considering that this type of structural system can be applied to both small buildings and larger structures, such as bridges. In this context, there is a wide variety in the thickness of the concrete slabs that make up the composite structures, and consequently, the height of the connector must adapt to these dimensions. In the case of the TTR connector with the geometric configuration of Barbosa (2016), its application is limited to composite beams with a concrete slab with a thickness of at least 150 mm, considering that the height of the connector is 130 mm. On the other hand, for application in slabs with a thickness greater than 150 mm, the behavior of the connector for this situation is not known. However, seeking to disseminate the applicability of the TTR connector, it is essential to evaluate the influence of the connector's height on its resistance capacity.

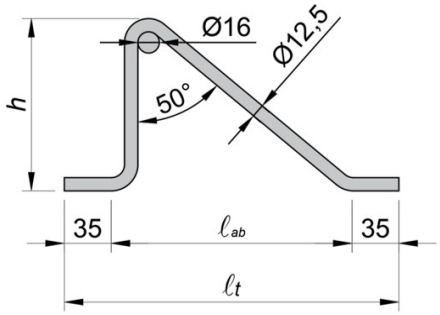

Figure 17 TTR connector geometric parameters – dimensions in cm

To verify the influence of the TTR connector height on its resistance capacity, push-out tests were simulated with the proposed finite element model on TTR connectors with a diameter of 12.5 mm and heights of 150 mm, 130 mm, 110 mm and 90 mm. These height values were defined with the aim of covering heights lower and higher than the connectors experimentally tested by Barbosa (2016). The other geometric parameters and concrete strength were kept constant. Table 5 presents the different heights analyzed and their respective nomenclature. Figure 18 shows the geometric configuration of each connector. For TTR-150 it was necessary to increase the height of the concrete slab to 175 mm, so that the minimum coverage was respected.

Table 5 Nomenclature of connectors for parametric study

Connector nomenclature	*h* (mm)
TTR-90	90
TTR-110	110
TTR-130	130
TTR-150	150

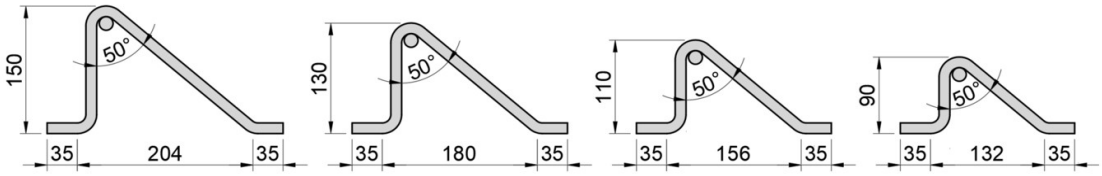

Figure 18 TTR connector geometry for each height– dimensions in mm

Figure 19 shows the load x slip curves for the push-out models with the TTR connectors described in Table 5. It is observed that up to a load of approximately 1000 kN, the behavior of the models is similar, with slips proportional to the

loads. From a load of 1000 kN onwards, there is a loss of stiffness in all models, however, the flow plateaus have different levels. To define the resistance capacity of the models, and consequently of the TTR connectors, the ultimate load of the models was defined for a sliding of 20.88 mm, the same criterion adopted in the validation of the numerical model. Figure 20 shows the resistance capacity of the models depending on the height of the TTR connectors. It is observed that there is an increase in the resistance capacity as the height of the connectors increases.

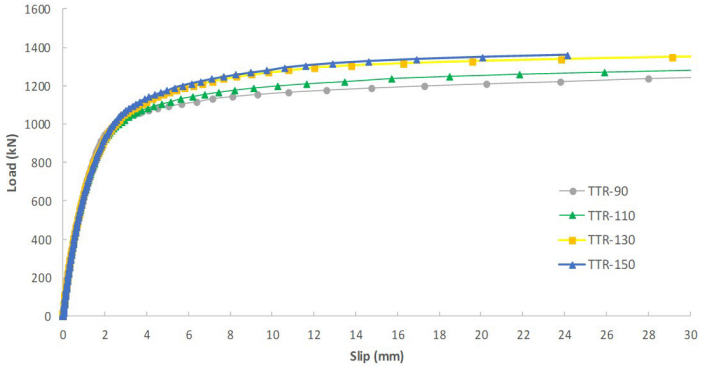

Figure 19 Load x slip curves for each TTR connector height

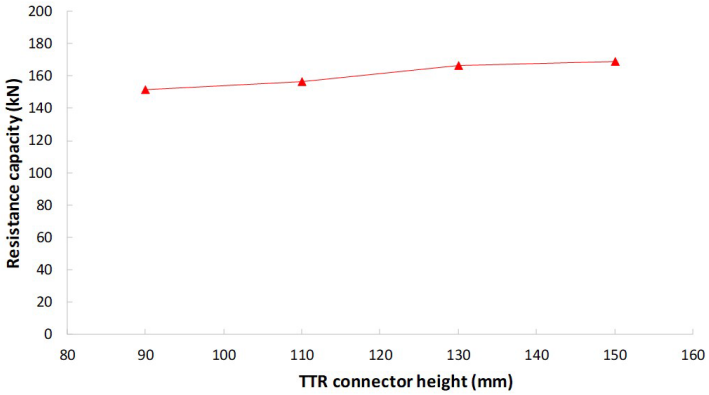

Figure 20 Resistance capacity for each height of the TTR connector

Table 6 presents the resistance capacity per connector, obtained by dividing the model's ultimate load value by 8 (number of connectors). The relationship between the resistance capacity of each TTR connector (P_{TTR}) and the resistance capacity of the TTR connector with a height of 130 mm (P_{TTR}) is also presented. The TTR-110 and TTR-90 connectors had a reduction in resistance capacity compared to the TTR-130 of 5.9% and 9.0%, respectively. These levels of resistance reduction indicate that the TTR connector has the potential to be applied to thinner slabs, that is, small composite structures. The TTR-150 did not have a significant gain in resistance capacity, just 1.4% compared to the TTR-130.

Table 6 Resistance capacity of TTR connectors for different heights

Connector	P_{TTR} (kN)	$P_{TTR}/P_{TTR-130}$
TTR-90	151.42	0.910
TTR-110	156.43	0.941
TTR-130	166.32	-
TTR-150	168.71	1.014

Figure 21 shows the deformed configuration and the Von Mises stress distribution for the analyzed models. It is observed that the deformed configuration of the TTR connectors is similar for all heights. Regarding stress distribution, for smaller connectors (90 mm and 110 mm), stresses greater than the yield stress of the steel is distributed throughout practically the entire connector, mainly in the vertical leg. For TTR connectors with heights of 130 mm and 150 mm, the

high stress levels are concentrated at the base of the connector. This justifies the small increase in resistance capacity of the TTR-150 in relation to the TTR-130, as can be seen in Figure 20 and Table 6.

5.1 Comparison between the TTR and TTI connectors

The resistance capacity results of the TTR connector were compared with the results of Lima et al. (2020), who numerically evaluated the resistance capacity of the TTI connector for different connector heights. Lima et al. (2020) simulated push-out models with TTI connectors with the respective heights evaluated in this study for the TTR connector. The mechanical properties of the steel and concrete of the models were also the same as those in this study. Table 7 shows the resistance capacity values of the TTR (P_{TTR}) and TTI (P_{TTI}) connectors and the P_{TTR}/P_{TTI} ratio for each height.

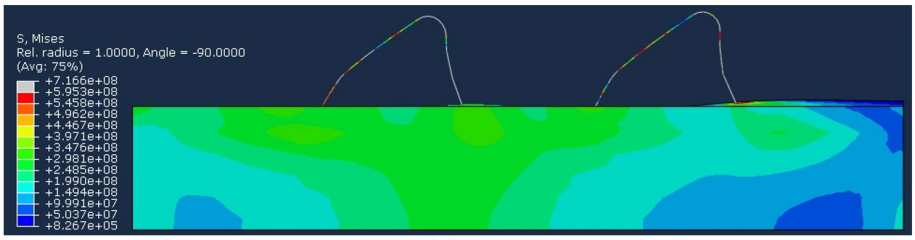

(a) TTR-90

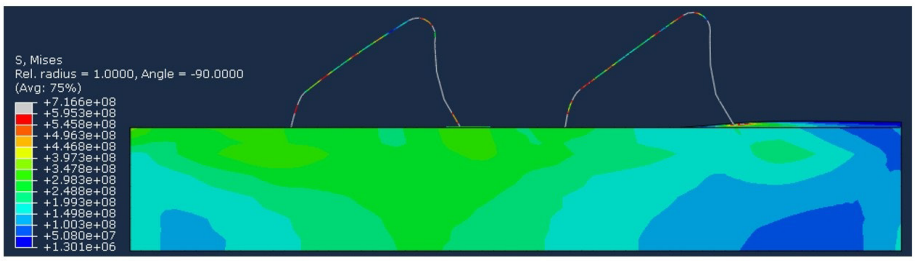

(b) TTR-110

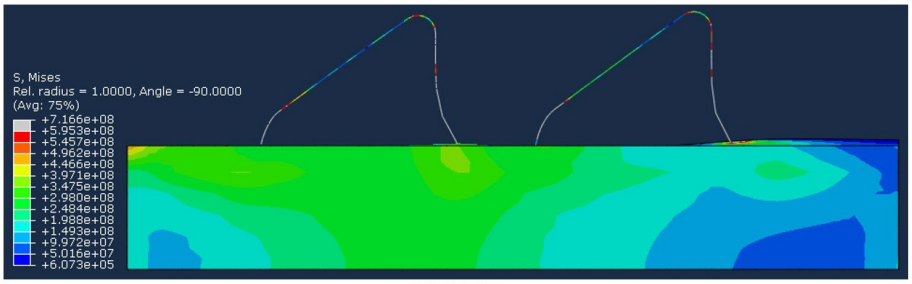

(c) TTR-130

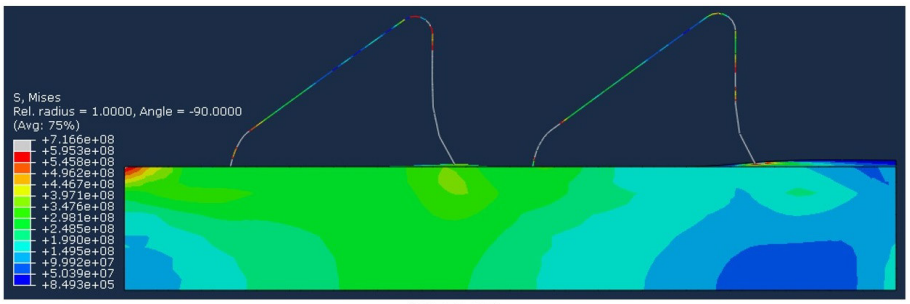

(d) TTR-150

Figure 21 Deformed configuration and the Von Mises stress distribution (Pa)

Table 7 Comparison between the resistance capacity of TTR and TTI connectors

Connector height	P_{TTR} (kN)	P_{TTI} (kN)	P_{TTR}/P_{TTI}
90	151.42	181.75	0.833
110	156.43	189.02	0.827
130	166.32	189.61	0.877
150	168.71	194.87	0.865

Just like the TTR connector, the resistance capacity of the TTI connector tends to increase with the increase in its height. On average, the TTR connector presented resistance capacity results 15% lower than the TTI connector. According to Barbosa (2016), Bezerra et al. (2018) and Lima et al (2020), the TTI connector has one of the legs that works predominantly on tensile efforts, which inhibits the effects of instability, thus giving greater efficiency to this configuration of the TT connector. However, based on the comparison made in Table 7, it can be considered that there is no significant difference between the resistance capacity of TTR and TTI connectors.

Figure 22 shows the resistance capacity results of the two configurations of the TT connector for different heights. For each set of results, a trend line was drawn from a linear regression. Equation 15 describes the adopted regression. The angular coefficients of the regressions of the TTR and TTR connectors were 0.199 and 0.307, respectively. In other words, the angular coefficient of the TTR connector is 35% greater than that of the TTI one, indicating that the effect of varying the height of the connector is more significant for the configuration of the TT connector studied in this research.

$$y = ax + b \tag{15}$$

y - Independent variable (connector resistance capacity)
x – Dependent variable (connector height)
a – Slope
b – Linear coeficiente

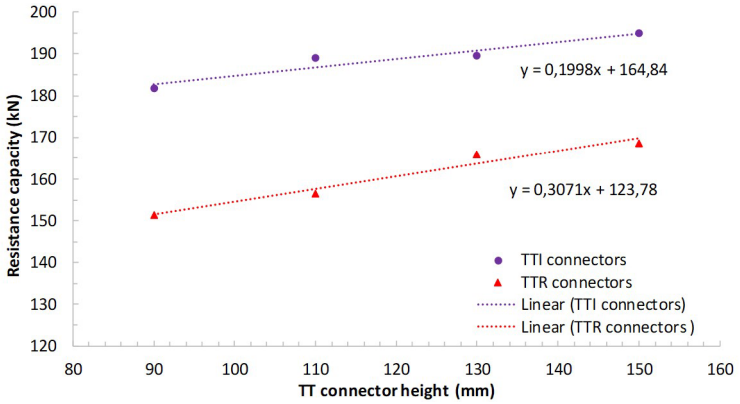

Figure 22 Evolution of resistance capacity with variation inTT connector height

6 CONCLUSIONS

A new approach for numerical modeling of the behavior of the Right-angle Truss-Type shear connector in the push-out test was presented in this work. In the finite element models built using the Abaqus software, the connectors were designed as linear elements. All sources of nonlinearities in materials and contact between elements were considered in the model. The Concrete Damage Plastic Model was used to represent the behavior of concrete and the analysis was carried out by the Dynamic Explicit Method.

Comparing the load-slip curves, it was possible to verify good convergence between the numerical results and the experimental results presented in Barbosa (2016). The ultimate load obtained by the finite element model was only 5.7% lower than the average load obtained experimentally. Furthermore, the failure mode observed in the numerical model was similar to the experimental one, in which there is a concentration of stress close to the connection of the TTR connector to the steel profile and crushing of the concrete in this region.

The use of linear finite elements in modeling TTR connectors resulted in a processing time of 45 minutes, while the models with three-dimensional finite elements developed by Lima et al. (2022) required 19 hours to process. On the other hand, the significant reduction in computational cost provided by the use of linear finite elements resulted in a loss of precision of only 1.01%, which does not compromise the quality of the result. Therefore, the proposed methodology proved to be efficient and very attractive, especially for carrying out robust parametric studies that require the construction of many models.

Furthermore, the use of linear finite elements in TTR connectors modeling did not affect the stress distribution in the connectors and in the concrete slab. It was observed that the modeled connector has a compressed leg and a bending

leg like the model with three-dimensional finite elements developed by Lima et al. (2022) and the experimental program by Barbosa (2016). Another similarity is also observed in the stress distribution in the slab. In both models, the concrete crushes in the region of the connector leg base.

From the study of the variation in the height of the TTR connector, it was possible to observe that the higher its value, the greater the resistance capacity. However, this increase in resistance is not significant and tends to decrease the higher the height. Among the models analyzed, the greatest increase in resistance was 8.78% and occurred between the two lowest heights (increase from 90 mm to 130 mm). Therefore, considering constructive aspects and association with thinner slabs, the 90 mm high TTR connector presented the best cost-benefit ratio. It is also worth noting that the resistance of the TTR connector increases with increasing height at a higher rate than the TTI connector.

ACKNOWLEDGMENT

The authors would like to thank FUNCAP (Cearense Foundation to Support Scientific and Technological Development) and CNPq (the National Council for Scientific and Technological Development) for the financial supports for this research.

Author's Contribuitions: Conceptualization: Luciano Mendes Bezerra, Jerfson Moura Lima and Ramon Silva; Investigation: Paulo Henrique Roberto Moura, Jerfson Moura Lima, Gustavo Henrique Silva Rodrigues and Eric Mateus Fernandes Bezerra; Methodology: Paulo Henrique Roberto Moura and Gustavo Henrique Silva Rodrigues; Supervision: Luciano Mendes Bezerra and Ramon Silva; Writing – original draft: Jerfson Moura Lima, Eric Mateus Fernandes Bezerra and Paulo Henrique Roberto Moura; Writing - review & editing: Jerfson Moura Lima, Ramon Silva and Luciano Mendes Bezerra.

Editor: Marco L. Bittencourt

REFERENCES

ABAQUS, User's Manual, Version 6.14-4. (2014). Dessault Systèmes Simulia Corp, Providence, RI, USA.

Alfarah, B., López-Almansa, F. and Oller, S. (2017), New methodology for calculating damage variables evolution in Plastic Damage Model for RC structures, Eng. Struct., 132, 70-86.

Barbosa, W. C. S. (2016). Study of shear connectors in steel bars for steel-concrete composite Beams, Ph.D. Thesis, University of Brasilia, Brazil.

Bezerra, L. M., Barbosa, W. C. S., Bonilla, J., Cavalcante, O. R. O. (2018). Truss-type shear connector for composite steel-concrete beams. Construction and Building Materials, v. 167, p. 757–767.

Bonilla, J., Bezerra, L. M., Mirambell, E. (2019). Resistance of stud shear connectors in composite beams using profiled steel sheeting. Engineering Structures, v. 187, p. 478–489.

Bonilla, J., Bezerra, L. M., Larrúa, R., Recarey, C., Mirambell, E. (2015). Numerical modeling with experimental validation applied to the study of the behavior of bolt-type connectors of composite structures of concrete and steel. Construction Engineering Journal, v. 30, n. 1, p. 53–68.

Cornelissen H., Hordijk D. and Reinhardt, H. (1986). Experimental determination of crack softening characteristics of normal weight and lightweight concrete, Heron. 31 45-56.

Eurocode-4 (2004), Design of Composite Steel and Concrete Structures Part 1.1; European Committee for Standardization, Brussels, Belgium.

Fib Model Code 2010 (2012), fib Model Code 2010 Final draft Volume 2, The International Federation for Structural Concrete, Lausanne, Switzerland.

Han, Q., Wang, Y., Xu, J., Xing, Y., Yang, G. (2017). Numerical analysis on shear stud in push-out test with crumb rubber concrete. Journal of Constructional Steel Research, v. 130, p. 148–158.

Kim, S. H., Kim, K. S., Park, S., Ahn, J. H., Lee, M. K. (2016). Y-type perfobond rib shear connectors subjected to fatigue loading on highway bridges. Journal of Constructional Steel Research, v. 122, p. 445–454.

KIM, S. H.; PARK, S.; KIM, K. S.; JUNG, C. Y. (2017). Generalized formulation for shear resistance on Y-type perfobond rib shear connectors. Journal of Constructional Steel Research, v. 128, p. 245-260.

Krätzig, W.B. and Pölling R. (2004). An elasto-plastic damage model for reinforced concrete with minimum number of material parameters, Comput. Struct., 82(15-16), 1201-1215.

Lacki, P., Nawrot, J., Derlatka, A., Winowiecka, J. (2019). Numerical and experimental tests of steel-concrete composite beam with the connector made of top-hat profile. Composite Structures, v. 211, p. 244-253.

Lima, J. M., Bezerra, L. M., Bonilla, J., Mirambell, E. (2024) Experimental study on full scale steel-concrete composite beams using truss-type shear connectors. Engineering Structures, v. 303, p. 117490.

Lima, J. M., Bezerra, L. M., Bonilla, J., Barbosa, W. C. S. (2022) Study of the behavior and resistance of right-angle truss shear connector for composite steel concrete beams. Engineering Structures, v. 253, p. 113778.

Lima, J. M. (2021). Experimental and numerical study of the behavior of steel-concrete composite beams with truss shear connector, Ph.D. Thesis, University of Brasilia, Brazil.

Lima, J. M., Bezerra, L. M., Bonilla, J., Silva, R. S. Y. R. C., Barbosa, W. C. S. (2020) Behavior and resistance of truss-type shear connector for composite steel-concrete beams. Steel and Composite Structures, v. 36, n. 5, p. 569–586.

Lopez-Almansa, F., Alfarah, B. and Oller, S. (2014), Numerical simulation of RC frame testing with damaged plasticity model comparison with simplified models. Proceedings of the Conference: 2nd European conference on earthquake engineering and seismology, Istanbul, Turkey, August.

Nguyen, H.T. and Kim, S.E. (2009). Finite element modeling of push-out tests for large stud shear connectors. J. Constr. Steel Res., 65(10-11), 1909-1920.

OLLER, S. (1988). A continuous damage model for frictional materials, Ph.D. Thesis, Polytechnic University of Catalonia, Barcelona, p. 471.

Qureshi, J., Lam, D. (2012). Behaviour of headed shear stud in composite beams with profiled metal decking. Advances in Structural Engineering, v. 15, n. 9, p. 1547–1558.

Qureshi, J., Lam, D., Ye, J. (2011). Effect of shear connector spacing and layout on the shear connector capacity in composite beams. Journal of Constructional Steel Research, v. 67, n. 4, p. 706–719.

Shariati, M., Ramlisulong, N. H., Shariati, A., Khanouki, M. A. (2016). Behavior of V-shaped angle shear connectors: experimental and parametric study. Materials and Structures, v. 49, n. 9, p. 3909–3926.

Xu, C., Su, Q., Sugiura, K. (2017). Mechanism study on the low cycle fatigue behavior of group studs shear connectors in steel-concrete composite bridges. Journal of Constructional Steel Research, v. 138, p. 196–207.

Xu, X., Liu, Y., He, J. (2014). Study on mechanical behavior of rubber-sleeved studs for steel and concrete composite structures. Construction and Building Materials, v. 53, p. 533–546.

Zheng, S., Liu, Y., Liu, Y. and Zhao, C. (2019). Experimental and parametric study on the pull-out resistance of a notched perfobond shear connector. Appl. Sci., 9(4), 1-20.